A Transfer Matrix Technique for Evaluating the Natural Frequencies and Critical Speeds of a Rotor With Multiple Flexible Disks

F. Wu
Lecturer,
Anhui Institute of Technology,
Hefei, Anhui, P.R. China

G. T. Flowers
Assistant Professor,
Department of Mechanical Engineering,
College of Engineering,
Auburn University,
Auburn, Alabama

The influence of disk flexibility on the rotordynamical behavior of turbomachinery is a topic that is of some concern to designers and analysts of such equipment. Research in this area has indicated that disk flexibility may significantly alter the dynamical behavior of a rotor system. This research effort is concerned with developing a procedure to account for disk flexibility which can readily be used for investigating how such effects might influence the natural frequencies and critical speeds of practical rotor systems. A transfer matrix procedure is developed in this work in which the disk flexibility effects are accounted for by means of additional terms included in the transfer matrix formulation. In this way the efficiency and practicality of the transfer matrix method is retained. To demonstrate this technique, a simple rotor system is studied for the effect of disk flexibility and the results discussed.

Introduction

Rotor systems have typically been modelled with the assumption that the bladed disks are much more rigid laterally than is the rotor shaft. As a result, little dynamical interaction is thought to occur between the two and the problems of disk dynamics and shaft dynamics can be treated separately. Rotor studies in which the effects of disk flexibility have been incorporated indicate that, under certain conditions, significant dynamical coupling may occur. Vance [1] has experimentally demonstrated that in certain cases disk flexibility may significantly alter rotordynamical behavior.

In the present work, the shaft is treated as a discrete system while the disk is modelled as a continuous system using the governing partial differential equation. A transfer matrix approach is then developed for the computation of the natural frequencies and critical speeds of rotors with multiple flexible disks. Using a model expansion method, disk flexibility effects are accounted for by means of additional terms included in a transfer matrix formulation of the rotor equations of motion. By so doing, the properties of quick computation speed and easy use are kept and the complexity of dividing disk into many elements or of solving partial differential equations is avoided. This leads to the present procedure which can be easily applied to practical engineering problems. This is especially true for multiple flexible disk rotors. Three different cases of disk flexibility for a multiple disk rotor have been studied using this procedure to demonstrate its usefulness in engineering practice and some interesting results are obtained.

Contributed by the Technical Committee on Vibration and Sound for publication in the JOURNAL OF VIBRATION AND ACOUSTICS. Manuscript received Sept. 1990.

Previous Work

The study of the vibration of shaft-disk systems has drawn the attention of investigators for many years. In 1919, Jeffcott presented a simple but important shaft-disk model for the study of rotordynamics. Using this model, the effects of various parameters on rotordynamical behavior, such as gyroscopic effects, rotary inertia and bearing stiffness, have been studied. Many methods [2], such as the boundary-value differential equation method, Rayleigh-Ritz method, Galerkin's method, transfer matrix method, finite elements method, etc. have been employed in these studies. However, almost all of these early studies considered the disk as a rigid structure.

On the other hand, the vibration of flexible spinning disks has received extensive study. The earliest analyses were by Lamb and Southwell [3], and Southwell [4]. In these two papers the natural frequencies and mode shapes of a solid circular disk and an annular disk were studied. The authors gave the results for a very flexible disk (neglecting bending stiffness) and a slowly rotating disk (neglecting membrane forces), as well as an approximate solution for the case when both bending stiffness and membrane forces are included. Since then, more complex configurations have been studied by numerous investigators. Among them are Eversman and Dodson [5], Hutchinson [6], Chonan [7], Adams [8], and many others. A more complete review of literature in this area can be found in Davis [9].

In recent years, the effects of disk flexibility on the dynamic behavior of shaft-disk systems have attracted the attention of investigators. The problem of a continuous shaft carrying a rigid disk has been studied by Ozguven [11], for the nonrotating case and by Eshleman and Eubanks [12], for the rotating case. For the case of a continuous shaft carrying a

flexible disk, Chivens and Nelson [13] discussed the natural frequencies and critical speeds, and Wilgen and Schlack, Jr. [14] studied its stability. In the above studies, the authors employed boundary-value differential equation methods. Other methods have also been used to investigate the effects of disk flexibility on the dynamic behavior of disk-shaft system. Dividing both shaft and disk into several segments, Dopkin and Shoup [15] developed a transfer matrix approach to include the effects of disk flexibility and gyroscopic forces, and studied the effects of rotating speed, disk stiffness and disk position on the first mode of a rotating shaft with one disk. Shahab and Thomas [16] used the finite element method with a special thick, three-dimensional cylindrical element to study the coupling effects of disk flexibility on the dynamic behavior of non-rotating multi disk-shaft system. Klompas [17] suggested a method which lumps the dynamic moment of each flexible disk into an equivalent gyroscopic moment. He introduced three parameters, I_{pn}, C_n^+ and C_n^-, to represent the dynamic characteristics of the disk. He assumed that these parameters are known quantities.

Analysis

1 Equations of Motion. Figure 1 shows the geometric configuration of the disk-shaft system which was used in the analysis for this paper. The system may consist of multiple disks. For clarity, Fig. 1 only shows the disk at kth station. The transverse bending displacements of the shaft can be expressed as

$$X=\tilde{X}(z)\cos\omega t$$
$$Y=\tilde{Y}(z)\sin\omega t \tag{1}$$

When $\tilde{X}(z) = \tilde{Y}(z)$, the motion of shaft center is circular and if $X(z)$ and $Y(z)$ are not the same, the motion will be elliptical. The angular displacements β and ψ are determined by

$$\beta=\frac{\partial X}{\partial z}=\frac{d\tilde{X}}{dz}\cos\omega t=\tilde{\beta}\cos\omega t$$
$$\psi=\frac{\partial Y}{\partial z}=\frac{d\tilde{Y}}{dz}\sin\omega t=\tilde{\psi}\sin\omega t \tag{2}$$

We can formulate the governing equation of motion for the bending of a thin circular plate disk by either the application of Newton's Second Law or of Hamilton's principle. With the assumption of small deflections, the equation of motion of the disk in terms of displacement w is

$$\rho\frac{\partial^2 w}{\partial t^2}+D\nabla^4 w-\frac{1}{r}\frac{\partial}{\partial r}\left(Pr\frac{\partial w}{\partial r}\right)-\frac{Q}{r^2}\frac{\partial^2 W}{\partial\theta^2}=-\rho\ddot{\psi}r\sin\theta$$
$$-\rho\ddot{\beta}r\cos\theta-2\rho\Omega\dot{\psi}r\cos\theta+2\rho\Omega\dot{\beta}r\sin\theta \tag{3}$$

Using the method of space-time separation of variables, we can express the harmonic time solution of w in the form

$$w=w_1(r,\theta)\sin\omega t+w_2(r,\theta)\cos\omega t=w_I+w_{II} \tag{4}$$

Substituting (4) and (2) into (3), we can separate (3) into two similar portions. One portion only includes w_I and the other only includes w_{II}. Because of the similarity of the two portions, we only consider w_I further in this paper and will omit the subscripts I, II and 1, 2. The equation is

$$\rho\frac{\partial^2 w}{\partial t^2}+D\nabla^4 w-\frac{1}{r}\frac{\partial}{\partial r}\left(Pr\frac{\partial w}{\partial r}\right)-\frac{Q}{r^2}\frac{\partial^2 w}{\partial\theta^2}$$
$$=\rho\left[\omega^2-2\Omega\omega\frac{\tilde{\beta}}{\tilde{\psi}}\right](r\sin\theta)\cdot\psi \tag{5}$$

2 Forces and Moments Analysis. Figure 2 shows the free body diagram of a flexible disk at the kth station in the y-z plane. The diagram in the x-z plane is similar and is not shown. The restoring forces and moments caused by the deformation of shaft and spring elements are V_k, M_k and K_kY_k. The inertia

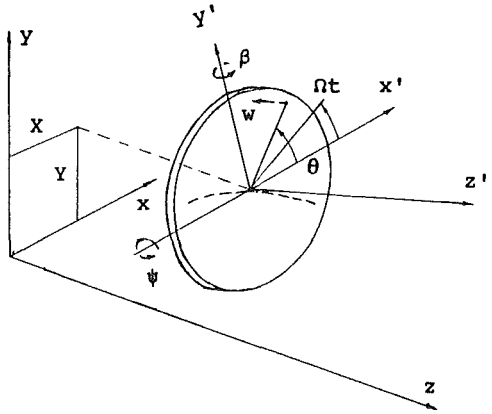

Fig. 1 Geometric configuration

Nomenclature

b = disk radius
c_i, c_r = coefficients
D = integration domain; plate flexural rigidity
E = Young's modulus
f = force function
h = disk thickness
I = area moment of shaft
I_d, I_p = mass inertial moments of rigid disk
k = spring constant
k_c = coefficients
m = mass
L = operator; length of shaft span
M = operator; elastic restoring moment
M_k^* = inertial moment
N_r, Q_r = generalized force function
p = spatial position
P, Q = disk radial and transverse in-plane stresses
q_i, $\{q\}$, $\{\nu\}$ = generalized coordinates
R_i, R_{ns} = disk bending displacement along radius
$\bar{R}_i$, $\{\bar{R}\}$ = coefficients
T = kinetic energy
$[u]$ = modal matrix
V = elastic restoring force; potential energy
w = disk bending displacement
w_1, w_2 = two parts of disk spacial bending displacement
w_I, w_{II} = two parts of disk bending displacement
w_{is}, w_{ns} = disk spacial bending displacement
X, Y = shaft transverse displacement
$\tilde{X}$, $\tilde{Y}$ = shaft spatial displacement
β, ψ = shaft angular displacement
$\tilde{\beta}$, $\tilde{\psi}$ = shaft spatial angular displacement
λ_i = frequency ratio
ν = Poisson's ratio
ρ = disk mass density
Ω = rotor spin speed
ω = circular natural frequency of system

Subscripts

d = disk
k = shaft station
L = left
R = right
s = shaft

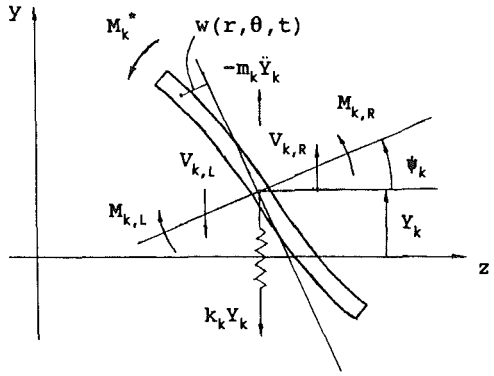

Fig. 2 Free body diagram

force of transverse motion is $-m_k\ddot{Y}_k$. To write the inertia moment M_k^*, consider the displacement of an elastic disk expressed in the general form according to expansion theory

$$w(r,\theta,t)=\sum_{i=1}^{\infty} w_i(r,\theta)q_i(t) \tag{6}$$

The $w_i(r, \theta)$ represent space-dependent functions, i.e. the mode shapes, and the $q_i(t)$ are generalized coordinates. Furthermore, the $w_i(r, \theta)$ can be written in the form [3]

$$w_i(r,\theta)=R_{ns}(r)\sin s\theta=w_{ns}(r,\theta) \tag{7}$$

where $w_{ns}(r, \theta)$ represent the mode shapes of n nodal circles and s nodal diameters. $w_i(r, \theta)$ can be thought as the reranking of $w_{ns}(r, \theta)$ by order of increasing correspondent natural frequency. Thus the inertia moment M_k^* is

$$M_k^*=-h\int\int\left[\frac{\partial^2 w}{\partial t^2}+(\psi-2\Omega\dot{\beta})r\sin\theta\right](r\sin\theta)\cdot\rho r dr d\theta \tag{8}$$

For harmonic motion, $\ddot{q}_i(t) = -\omega^2 q_i$, $\dot{\psi} = -\omega^2\psi$, $\dot{\beta} = -\omega\,\tilde{\beta}/\tilde{\psi}\,\psi$. The above equation can be written as

$$M_k^*=h\omega^2\sum_{i=1}^{\infty} q_i(t)\int\int R_{ns}(r)\sin s\theta\cdot\sin\theta\cdot r^2\rho dr d\theta + \frac{b^2}{4}m_d\psi\cdot\omega^2-\frac{b^2}{2}m_d\psi\Omega\omega\cdot\frac{\tilde{\beta}}{\tilde{\psi}} \tag{9}$$

One can notice that

$$\int\int R_{ns}(r)\sin s\theta * \sin\theta * r^2 dr d\theta=\begin{cases}\pi\int R_{n1}(r)r^2 dr & \text{for } s=1\\ 0 & \text{for } s\neq 1\end{cases} \tag{10}$$

This means that only the modes of one nodal diameter give the contribution to inertia moment M^*. Denoting $R_{n1}(r)$ by $R_i(r)$, we have

$$M_k^*=h\rho\pi\omega^2\sum_{i=1}^{\infty} q_i(t)\int R_i(r)r^2 dr + I_{dk}\omega^2\psi_k-I_{pk}\Omega\omega\cdot\frac{\tilde{\beta}}{\tilde{\psi}}\cdot\psi_k \tag{11}$$

I_d is the moment of inertia of the rigid disk about its diameter, and I_p is the moment of inertia about its spin axis. For the case of circular motion of the shaft center, $\tilde{\beta}/\tilde{\psi} = 1$.

3 Determination of Inertia Moment M_k^*. To determine the $q_i(t)$, the operators M and L can be used to write Eq. (5), as well as its solution Eq. (1), into a short form with p representing the spatial position.

$$M\frac{\partial^2 w}{\partial t^2}+L[w]=f \tag{12}$$

$$w(p,t)=\sum_{r=1}^{\infty} w_r(p)q_r(t) \tag{13}$$

Substitution of (13) into (12), yields

$$\sum_{r=1}^{\infty}\ddot{q}_r(t)Mw_r(p)+\sum_{r=1}^{\infty} q_r(t)L[w_r(p)]=f(p,t) \tag{14}$$

Multiplication of Eq. (14) by $w_s(p)$ and integration over the domain D yields

$$\sum_{r=1}^{\infty}\ddot{q}_r(t)\int_D w_s(p)Mw_r(p)dD + \sum_{r=1}^{\infty} q_r(t)\int_D w_s(p)L[w_r(p)]dD=\int_D w_s(p)f(p,t)dD \tag{15}$$

Application of orthogonality conditions for the mode shapes to (15) produces

$$\ddot{q}_r(t)+\omega_r^2 q_r(t)=N_r(t)\quad r=1,2,\ldots \tag{16}$$

where

$$N_r(t)=\int_D w_r(p)f(p,t)dD\quad r=1,2,\ldots \tag{17}$$

are the generalized forces. For the case of harmonic excitation, substitution of the force term in Eq. (5)

$$f=\rho\left[\omega^2-2\Omega\omega\frac{\tilde{\beta}}{\tilde{\psi}}\right]\psi r\sin\theta$$

into Eq. (17) yields

$$N_r=\omega^2\cdot c_r\cdot\psi \tag{18}$$

where

$$c_r=\rho\left(1-2\frac{\Omega}{\omega}\frac{\tilde{\beta}}{\tilde{\psi}}\right)\int_D w_r(p)r\sin\theta dD \tag{19}$$

Substituting (18) into (16), considering harmonic motion, gives the steady state responses

$$q_r(t)=c_r\cdot\frac{(\omega/\omega_r)^2}{1-(\omega/\omega_r)^2}\cdot\psi=c_r\frac{\lambda_r^2}{1-\lambda_r^2}\psi\quad r=1,2,\ldots \tag{20}$$

Substitution of (20) into (11) gives the inertia moment of the disk

$$M_k^*=(1+k_{ck})\cdot I_{dk}\omega^2\psi_k-I_{pk}\Omega\omega\cdot\frac{\tilde{\beta}}{\tilde{\psi}}\psi_k \tag{21}$$

where

$$k_{ck}=\frac{h\rho\pi}{I_{dk}}\sum_{1}^{\infty} c_i\cdot\frac{\lambda_i^2}{1-\lambda_i^2}\int R_i(r)r^2 dr \tag{22}$$

4 Point Transfer Matrix Including Disk Flexibility Effects. Having developed an expression for the inertia moment M_k^*, we can now obtain the kth point transfer matrix from Fig. 1

$$T_{pk}=\begin{bmatrix}1 & 0 & 0 & 0\\ 0 & 1 & 0 & 0\\ 0 & -(1+k_c)\cdot I_d\omega^2+I_p\Omega\omega\dfrac{\tilde{\beta}}{\tilde{\psi}} & 1 & 0\\ m\omega^2-k & 0 & 0 & 1\end{bmatrix} \tag{23}$$

This transfer matrix can serve for the case of circular whirling motion, where $\tilde{\beta}/\tilde{\psi} = 1$, and for the case of elliptical whirling motion for which the ratio $\tilde{\beta}/\tilde{\psi}$ is known. The transfer matrix for the case of arbitrary elliptical whirling motion will be discussed in another paper.

5 Assumed Modes Method. In practice the mode shape of a disk is approximated using comparison functions or admissible functions, or using data from numerical analyses or experimental tests. The displacement is then represented as

$$w(p,t)=\sum_{i=1}^{n} w_i(p)q_i(t) \tag{24}$$

Using this expression, the continuous system can be treated as an n-degree-of-freedom system. If only the approximate mode shapes and the stiffness properties of the disk are known, Eq. (22) cannot be used to obtain k_{ck}. One possible approach is to calculate the kinetic energy and potential energy of the disk in the form

$$T(t)=\frac{1}{2}\sum_{i=1}^{n}\sum_{j=1}^{n}m_{ij}\dot{q}_i(t)\dot{q}_j(t) \tag{25}$$

and

$$V(t)=\frac{1}{2}\sum_{i=1}^{n}\sum_{j=1}^{n}k_{ij}q_i(t)q_j(t) \tag{26}$$

where the m_{ij} depend on the mass distribution and mode shape of the disk, and the k_{ij} depend on the stiffness properties and mode shape of the disk. Lagrange's equations

$$\frac{d}{dt}\left(\frac{\partial T}{\partial \dot{q}_r}\right)-\frac{\partial T}{\partial q_r}+\frac{\partial V}{\partial q_r}=Q_r \quad r=1,2,\ldots,n \tag{27}$$

together with Eqs. (25) and (36) lead to the equation of motion of disk in matrix form

$$[m]\{\ddot{q}(t)\}+[k]\{q(t)\}=\{Q(t)\} \tag{28}$$

where

$$Q_i(t)=\int_D f(p,t)w_i(p)dD \tag{29}$$

Substituting the force term in Eq. (5) into (29) yields

$$Q_i(t)=\omega^2 c_i\psi \tag{30}$$

where

$$c_i=\rho\left(1-2\frac{\Omega}{\omega}\frac{\bar{\beta}}{\bar{\psi}}\right)\int\int w_i(r,\theta)r\sin\theta\cdot h r dr d\theta \tag{31}$$

For the case of harmonic excitation of $Q_i(t)$ with the frequency ω, the steady state solution of Eq. (28) is in the form

$$\{q\}=[u]\{\eta\} \tag{32}$$

Substitution (32) into (28), and premultiplication by $[u]^T$, yields

$$\{\ddot{\eta}\}+[\ddots\ \omega_i^2\ \ddots]\{\eta\}=[u]^T\{Q(t)\}=[u]^T\{c\}\omega^2\psi \tag{33}$$

from which we obtain

$$\{\eta\}=\left[\ddots\ \frac{\lambda_i^2}{1-\lambda_i^2}\ \ddots\right][u]^T\{c\}\psi \tag{34}$$

and

$$\{q\}=[u]\{\eta\}=[u]\left[\ddots\ \frac{\lambda_i^2}{1-\lambda_i^2}\ \ddots\right][u]^T\{c\}\psi \tag{35}$$

where

$$\lambda_i^2=\frac{\omega^2}{\omega_i^2} \tag{36}$$

are the non-dimensional frequencies.

Substitution of (35) into (11) yields M_k^* in a form similar to that of Eq. (24) with

$$k_c=\frac{h\rho\pi}{I_d}\sum_{i=1}^{n}\sum_{j=1}^{n}\sum_{k=1}^{n}\frac{\lambda_j^2}{1-\lambda_j^2}u_{ij}u_{jk}c_k\cdot\int R_i(r)r^2dr \tag{37}$$

Denoting

$$\bar{R}_i=\int R_i(r)r^2dr$$

and

$$\{\bar{R}\}=\{\bar{R}_1,\bar{R}_2,\ldots,\bar{R}_n\}^T$$

we can rewrite Eq. (37) into the matrix form

$$k_c=\frac{h\rho\pi}{I_d}\{\bar{R}\}^T[u]\left[\ddots\ \frac{\lambda_i^2}{1-\lambda_i^2}\ \ddots\right][u]^T\{c\} \tag{38}$$

Using Eq. (38), the point transfer matrix can then be formed.

Example Rotor System

Let us consider the Space Shuttle Main Engine (SSME) High Pressure Oxygen Turbo-pump (HPOTP) rotor as an example to demonstrate the effects of disk flexibility on the natural frequencies and the critical speeds of a rotor system. Consider that the disk at station 14 is flexible and that the rotor disks at other stations are rigid. The disk at station 14 represents a simplified model for the second turbine stage, which is the most flexible of the HPOTP rotor disks [18]. Figure 3 shows the nodal configuration of the simplified HPOTP rotor.

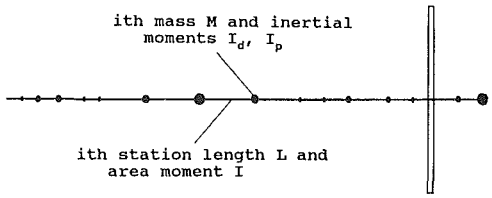

Fig. 3 The simplified nodal configuration of the HPTOP rotor

Only the 0 modal circle, 1 modal diameter mode is considered because in practice it represents the gravest vibration mode of a disk clamped at its center [3] [14]. This mode represents the vibration antisymmetric to the disk modal diameter and is the only one which contributes a coupling dynamic moment to the shaft.

To this end, we chose the simple admissible function

$$w(r,\theta,t)=\left(\frac{r}{b}\right)^2\sin\theta\cdot q(t) \tag{39}$$

to represent the disk's deformation. The disk is considered to be uniform. The kinetic energy of the disk is

$$2T(t)=\int\int M(r,\theta)\cdot\left(\frac{\partial w}{\partial t}\right)^2\cdot h r dr d\theta=m\cdot\dot{q}^2(t) \tag{40}$$

where

$$m=\frac{h\pi\rho b^2}{6} \tag{41}$$

The potential energy consists of two parts. The first is due to centrifugal forces

$$2V_1(t)=\int\int\left[P\left(\frac{\partial w}{\partial r}\right)^2+Q\left(\frac{\partial w}{r\partial\theta}\right)^2\right]\cdot h r dr d\theta \tag{42}$$

and the second is due to the flexural stiffness of the disk

$$2V_2(t)=D\int\int\left\{(\nabla^2 w)^2+2(1-\nu)\left[\left(\frac{1}{r}\frac{\partial^2 w}{\partial r\partial\theta}-\frac{1}{r^2}\frac{\partial w}{\partial\theta}\right)^2-\frac{\partial^2 w}{\partial r^2}\left(\frac{1}{r^2}\frac{\partial^2 w}{\partial\theta^2}+\frac{1}{r}\frac{\partial w}{\partial r}\right)\right]\right\}\cdot h r dr d\theta \tag{43}$$

$$P=A(b^2-r^2)\rho\Omega^2,\quad Q=(Ab^2-Br^2)\rho\Omega^2 \tag{44}$$

are the in-plane tensions of the disk, where

$$A=\frac{1}{8}(3+\nu),\quad B=\frac{1}{8}(1+3\nu),\quad D=\frac{Eh^2}{12(1-\nu^2)} \tag{45}$$

It is assumed in Eqs. (44) that the shaft is 'slender' with respect to the flexible disk. Such an assumption is in keeping with related developments of other researchers, most notably Southwell [4] and Chivens and Nelson [13]. For cases in which this assumption is poor, expressions for the radial and circumferential stress due to centrifugal loading should be derived taking into account the specific geometry of the disk/shaft coupling.

Substitution of (39) into (42) and (43), yields

$$2V_1(t)=\frac{\rho\Omega^2 h\pi b^2}{96}(19+\nu)\cdot q^2(t) \tag{46}$$

and

$$2V_2(t)=\frac{Eh^3\pi}{24(1-\nu^2)b^2}(7+2\nu)\cdot q^2(t) \tag{47}$$

The total potential energy of the disk is obtained by adding Eqs. (46) and (47) together.

$$2V(t) = 2V_1(t) + 2V_2(t) = k \cdot q^2(t) \tag{48}$$

where

$$k = \left[\frac{\rho \Omega^2 h \pi b^2}{96} (19 + \nu) + \frac{E h^3 \pi}{24(1-\nu^2)b^2} (7 + 2\nu) \right] \tag{49}$$

With the assumption of a circular orbit of the shaft center, $\tilde{\psi} = \tilde{\beta}$ and the generalized force applied on the disk in the direction of $q(t)$ will be

$$Q(t) = \rho(\omega^2 - 2\Omega\omega)\psi \int\int (r\sin\theta) \cdot \left(\frac{r^2}{b^2} \sin\theta \right) \cdot h r dr d\theta$$

$$= \frac{1}{5} \rho \pi b^3 h (\omega^2 - 2\Omega\omega)\psi \tag{50}$$

Combining Eqs. (40), (48) and (50) together, the equation of motion of the disk is

$$\ddot{q}(t) + \omega_n^2 q(t) = \omega^2 c \psi(t) \tag{51}$$

$$\omega_n^2 = \frac{\Omega^2}{16} (19 + \nu) + \frac{E h^2}{4\rho b^4} \cdot \frac{7 + 2\nu}{(1 - \nu^2)} \tag{52}$$

is the square of the natural frequency of the disk, and

$$c = \frac{6}{5} b \left(1 - 2 \frac{\Omega}{\omega} \right) \tag{53}$$

Considering both the excitation $\psi(t)$ and the response $q(t)$ to be harmonics of frequency ω, it follows that

$$q(t) = \frac{\lambda^2}{1 - \lambda^2} c \cdot \psi(t) \tag{54}$$

where $$\lambda^2 = \frac{\omega^2}{\omega_n^2}$$

With the calculation of

$$R = \int \left(\frac{r}{b} \right)^2 r^2 dr = \frac{1}{5} b^3 \tag{55}$$

we have

$$k_c = \frac{h\rho\pi}{\frac{h\rho\pi}{4} b^4} \cdot \frac{1}{5} b^3 \cdot \frac{6}{5} b \left(1 - 2 \frac{\Omega}{\omega} \right) \frac{\lambda^2}{1 - \lambda^2} = \frac{24}{25} \cdot \frac{\lambda^2}{1 - \lambda^2} \left(1 - 2 \frac{\Omega}{\omega} \right) \tag{56}$$

Discussion of Results

The influence of disk flexibility of the natural frequencies and critical speeds on an example rotor system (the SSME HPOTP) was evaluated in order to demonstrate the practicality of the procedure developed in this work. Three different disk stiffnesses have been used to compute the natural frequencies of the rotor as a function of rotor speed. The results of natural frequency versus rotor speed have been plotted in Fig. 4 through Fig. 6. In these three figures, dot lines represent the natural frequencies for an equivalent model with a rigid disk, while the solid lines represent the natural frequencies for the flexible disk rotor model. The modal shapes corresponding to the model in Fig. 5 have been plotted in Fig. 7 through Fig. 9. Figure 7 shows the modal shapes of rigid disk rotor. Figure 8 gives the modal shapes of the flexible disk rotor at operating speed. Figure 9 shows the modal shapes at a speed the third bending mode disappeared. From these six figures some interesting observations can be made.

(1) Rotor disk flexibility can lead to additional natural frequencies of the rotor system. At certain rotor speeds, there are nine natural frequencies for the rotor with a flexible disk and only eight for the rotor with rigid disk. If we consider more flexible disks and higher order mode shapes, there may be more additional natural frequencies. These additional frequencies are due to the coupling of disk motion with the motion of the rotor shaft.

(2) For forward whirling (shaft whirling direction is the same as the rotating direction), in the rotor speed range $\Omega < 1/2\ \omega_r$, the natural frequencies of the rotor with a flexible disk which are higher than the disk bending modal frequency are higher than those of the rotor with a rigid disk. For the natural frequencies which are lower than the disk bending modal frequency, those of the rotor with a flexible disk are lower than the ones of the rotor with a rigid disk. As rotor speeds increase, the differences in natural frequencies between the rigid disk rotor model and the flexible disk rotor model for all modes tends to decrease. In the rotor speed range $1/2\ \omega_r < \Omega < \omega_r$, the natural frequencies of the rotor with a flexible disk decrease rapidly while Ω increases. When $\Omega > \omega_r$, the natural frequencies of rotor with flexible disk tend to the next lower order ones of the rotor with a rigid disk.

(3) For backward whirling (shaft whirling direction is opposite to the rotating direction), the natural frequencies of the

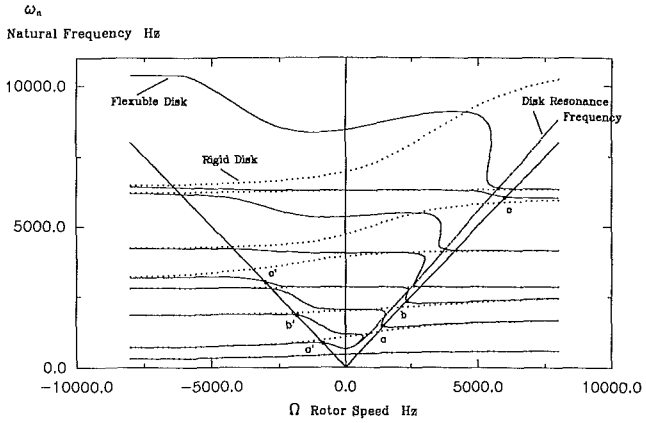

Fig. 4 Natural frequency versus rotor speed E_d = 5.175e10, E_s = 2.07e11

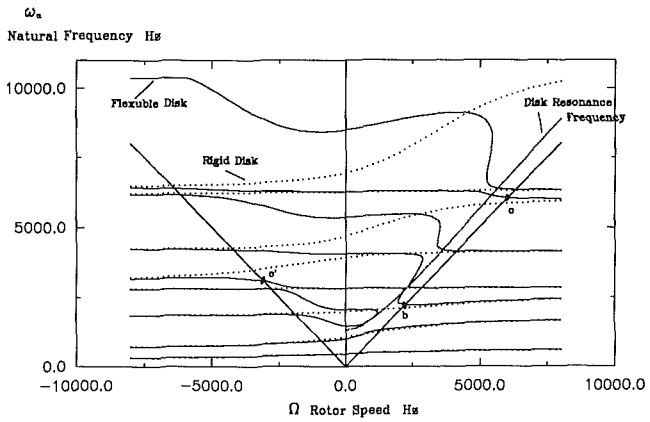

Fig. 5 Natural frequency versus rotor speed E_d = 2.07e11, E_s = 2.07e11

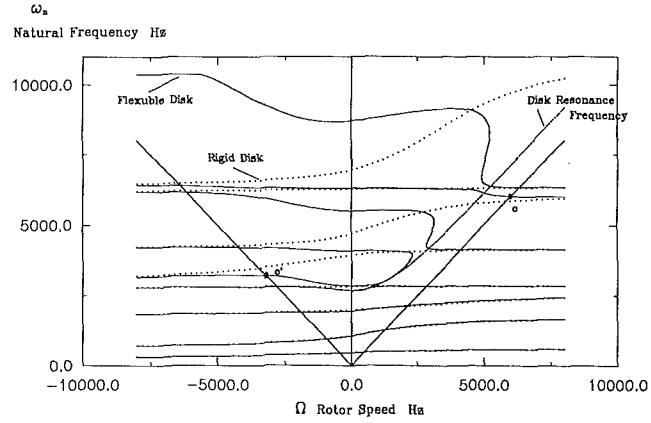

Fig. 6 Natural frequency versus rotor speed E_d = 8.28e11, E_s = 2.07e11

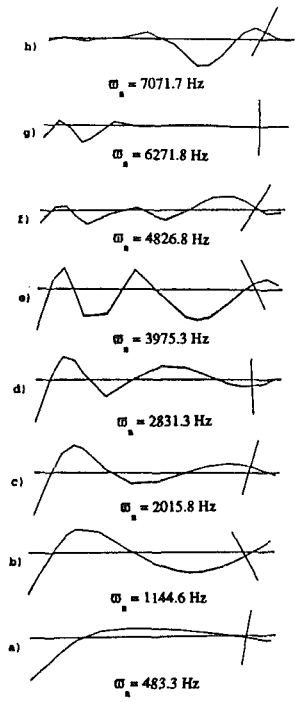

Fig. 7 Mode shape—rigid disk, Ω = 470 Hz, E_d = 2.07e11, E_s = 2.07e11

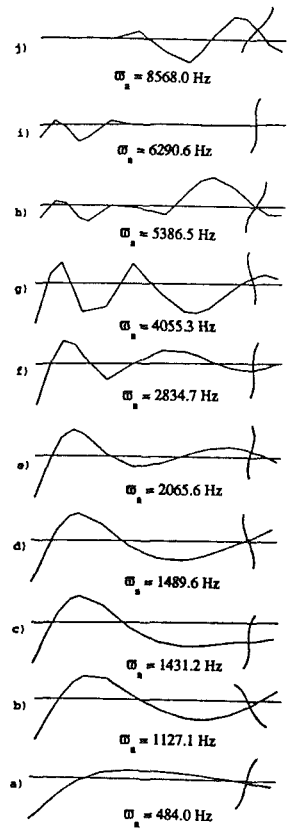

Fig. 8 Mode shape—flexible disk, Ω = 470 Hz, E_d = 2.07e11, E_s = 2.07e11

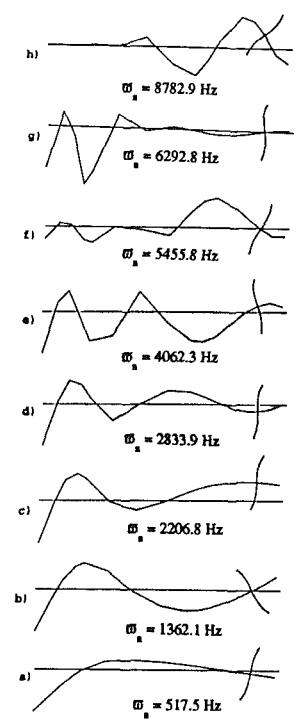

Fig. 9 Mode shape—flexible disk, Ω = 1600 Hz, E_d = 2.07e11, E_s = 2.07e11

rotor with a flexible disk increase and tend to the next higher order natural frequencies of the rotor with a rigid disk as rotor speed Ω increases.

(4) As disk flexibility is increased, lower order natural frequencies of a rotor-disk system will be more greatly effected. This is due to the disk natural frequencies coupling with the shaft frequencies at lower natural frequencies due to the increased disk flexibility.

(5) At particular rotor speeds, the disk flexibility may cause certain natural frequencies which exist in the rigid disk rotor model to disappear. For example, in Fig. 5 at the rotor speed around 1.5 Khz, the third natural frequency of the rotor with a rigid disk no longer exists in the rotor system with a flexible disk. This is because at this rotor speed the natural frequency of the rotor with a rigid disk is almost equal to the natural frequency of the disk mode itself. Thus, the disk acts as a dynamic vibration absorber and the rotor mode is eliminated.

(6) Figure 7 through Fig. 9 shows the modal shape of the rotor of which the natural frequencies are shown in Fig. 5. Figure 8(*c*) and Fig. 9(*c*) are the modal shape at disk resonance frequency. For such modes the large disk vibration amplitude takes most of the vibration energy and thus the shaft vibration amplitude must be small.

(7) For a particular mode, if the disk position is at a location where the shaft slope is small [either between modal nodes [Fig. 7(*d*)] or the local vibration is small [Fig. 7(*g*)]], the disk flexibility has little influence on the natural frequency of this mode. However, if the shaft slope is large at the disk position [[Fig. 7(*f*)] and [Fig. 7(*h*)]], then the disk flexibility can have considerable influence.

Conclusion

Most rotordynamical models are developed with the assumption that disks can be adequately modelled using rigid masses and inertias. In many cases, such models are quite adequate. However for cases in which one or more of the rotor disks may exhibit significant flexing, the rigid disk assumption can be quite poor and lead to significant error in analysis results. A common procedure for the analysis of natural frequencies and critical speeds in rotordynamics is the transfer matrix method. This study presents the development of rotordynamical equations that incorporate the effects of disk flexibility into a transfer matrix formulation. The derivation of these equations has been discussed in some detail and the associated assumptions and limitations noted. The results of this work make it possible for researchers in rotordynamics to modify current rigid disk rotordynamical analysis programs to include disk flexibility in a relatively easy and straightforward manner. An example case is presented in which the rotordynamics of the SSME HPOTP is studied for the effects of rotor disk flexibility and some interesting conclusions are drawn.

References

1 Vance, J. M., *Rotordynamics of Turbomachinery*, New York, Wiley, 1988.

2 Meirovitch, L., *Analytical Methods in Vibration*, New York, Macmillan, 1967.

3 Lamb, H., and Southwell, R. V., "The Vibration of a Spinning Disk," *Proceedings of the Royal Society*, London, Series A, Vol. 99, July 1921, pp. 272–280.

4 Southwell, R. V., "On the Free Transverse Vibrations of a Uniform Circular Disc Clamped at its Center; and on the Effects of Rotation," *Proceedings of the Royal Society*, London, Series A, Vol. 101, May 1922, pp. 133–153.

5 Eversman, W., and Dodson, R. O., "Free Vibration of a Centrally Clamped Spinning Circular Disk," *AIAA Journal*, Vol. 7, No. 10, Oct. 1969, pp. 2010–2012.

6 Hutchinson, J. R., "Vibration of Thick Free Circular Plates, Exact Versus Approximate Solutions," ASME *Journal of Applied Mechanics*, Vol. 51, Sept. 1984, pp. 581–585.

7 Chonan, S., "On the Critical Speed of a Rotating Circular Plates," ASME *Journal of Applied Mechanics*, Vol. 54, Dec. 1987, pp. 967–968.

8 Adams, G. G., "Critical Speeds for a Flexible Spinning Disk," *International Journal of Mechanical Science*, Vol. 29, No. 8, pp. 525–531, 1987.

9 Davis, R. R., "Practical Nonlinear Simulation of Rotating Machinery

Dynamics with Application to Turbine Blade Rubbing," Ph.D. Dissertation, Department of Mechanical Engineering, University of California, Davis, June 1989.

10 Sinha, S. K., "On Free Vibrations Of a Thin Spinning Disk Stiffened With an Outer Reinforcing Ring," ASME JOURNAL OF VIBRATION, ACOUSTICS, STRESS, AND RELIABILITY IN DESIGN, Vol. 110, Oct. 1988, pp. 507-514.

11 Özgüven, H. N., "On the Critical Speed of Continuous Shaft-Disk Systems," ASME JOURNAL OF VIBRATION, ACOUSTICS, STRESS, AND RELIABILITY IN DESIGN, Vol. 106, Jan. 1984, pp. 59-61.

12 Eshleman, R. L., and Eubanks, R. A., "On the Critical Speeds of a Continuous Shaft-Disk System," ASME *Journal of Engineering for Industry*, Vol. 89, Nov. 1967, pp. 645-652.

13 Chivens, D. R., and Nelson, H. D., "The Natural Frequencies and Critical Speeds of a Rotating, Flexible Shaft-Disk System," ASME *Journal of Engineering for Industry*, Vol. 97, No. 3, Aug. 1975, pp. 881-886.

14 Wilgen, F. J., and Schlack, Jr., A. L., "Effects of Disk Flexibility on Shaft Whirl Stability," ASME *Journal of Mechanical Design*, Vol. 101, April 1979, pp. 298-303.

15 Dopkin, J. A., and Shoup, T. E., "Rotor Resonant Speed Reduction Caused by Flexibility of Disks," ASME *Journal of Engineering for Industry*, Vol. 96, Nov. 1974, pp. 1328-1333.

16 Shahab, A. A. S., and Thomas, J., "Coupling Effects of Disc Flexibility on the Dynamic Behaviour of Multi Disc-Shaft Systems," *Journal of Sound and Vibration*, Vol. 114, No. 3, 1987, pp. 435-452.

17 Klompas, N., "Theory of Rotor Dynamics With Coupling of Disk and Blade Flexibility and Support Structure Asymmetry," ASME Paper No. 74-GT-159, ASME Gas Turbine Conference and Products Show, Zurich, Switzerland, March 30-April 4, 1974.

18 Flowers, G. T., "Effects of Rotor Disk Flexibility on the Rotordynamics of the Space Shuttle Main Engine Turbopumps," AIAA/ASME/ASCE/AHS/ASC 31st Structures, Structural Dynamics, and Materials Conference, Long Beach CA, April 2-4, 1990, pp. 2206-2213.